Chapter 3:

Studies of Guest Copper Schiff-base Complexes Entrapped in Zeolite Y and their Catalytic Activity for the Styrene Oxidation Reaction

***Abstract**: On encapsulation inside the supercage of zeolite-Y planar Cu(II)–Schiff base complexes show the modified structural, optical and functional properties. The electronic effect of the different substituent groups present in the catalyst plays the decisive role towards their reactivity in the homogeneous phase but after the encapsulation in zeolite Y, reactivity is mainly governed by the molecular dimensions of the guest complexes rather than the electronic factor of the substituent groups attached on them. These systems are well characterized with the help of different characterization tools like XRD analysis, SEM-EDX, AAS, FTIR, XPS, DSC, TGA, BET and UV–Visible spectroscopy and the comparative optical and catalytic studies have provided a rational explanation of enhanced reactivity of zeolite encapsulated metal complexes for various oxidation reactions compared to their corresponding solution states.*

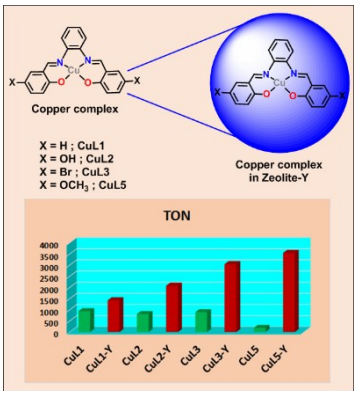

***S. Kumari**, A. Choudhary and S. Ray, *Appl. Organomet. Chem.*, 2019, **33**, e4765.

3.1 INTRODUCTION

Transformation of hydrocarbons into their oxy-functionalized derivatives are the important chemical processes for the industrial and academic purpose. Transition metal complexes are usually efficient catalysts for the oxidation of various organic compounds in mild reaction conditions; however, these homogeneous catalysts always have some drawbacks in the catalytic process like their instability, difficulty in the separation, and lack of reusability.[1-3]

The state-of-the-art of the catalytic science prefers such type of catalysts, which can overcome the limitations of the homogeneous catalytic processes without the loss of reactivity. Towards this direction, heterogenization of the homogeneous catalyst is a convenient approach to couple the reactivity of the complex with the stability with specific environment, thermal stability and ease of separation extended by host materials. There are many methods used for the purpose such as impregnation and encapsulation of transition metal complexes in the microporous,[4-12] mesoporous materials[13, 14] and MOFs.[15, 16,17] Homogeneous catalyst tagged with ionic liquids,[18, 19,20] alumina-supported metal complexes[21] and phase transfer catalyst[22, 23] are some interesting examples of heterogeneous systems, which have been successfully employed in the various oxidation reactions by using H_2O_2, TBHP, and molecular O_2 as oxidants.[24-30] Zeolites, the microporous aluminosilicate materials are the competent hosts for the encapsulation of transition metal complexes having the molecular dimension comparable with the diameter cavities of the host zeolites.[6, 31-36] These contemporary classes of catalysts comprise of the catalyst molecule encapsulated within the well-structured architecture of the host, with a large surface area. This is undoubtedly a unique way of achieving site isolation of the desired catalyst. These systems have shown a structural and functional analogy with cytochrome P450,[37]and are well explored as the proficient catalysts for the selective oxidative transformation of olefinic C-H bonds to its oxy-derivatives. Reasoning behind the enhancement of the catalytic activity of the encapsulated guest complex always remains underlying rationale for this research to explore. P. Ratanasmy and co-workers have mentioned about the structural distortion of both copper salen and 5-chloro copper salen complexes, encapsulated within zeolite Y while reporting them as efficient catalysts for the oxidation of p-xylene and phenol. The authors also emphasize upon the fact that the presence of electron withdrawing group on the phenyl rings immensely improves the TOF for the oxidation reaction.[2]

Few more reports are available in the literature, which also recognize the distorted geometry of the guest complex under space constraint imposed by the zeolite framework appears to be the one of the fundamental reasons for enhanced reactivity of the encapsulated complex. Maurya M. R *et al*. have studied catalytic activities of different metal complexes encapsulated in zeolite Y for oxidation of different hydrocarbons such as styrene, cyclohexane, cyclohexene, and methyl phenyl sulfide, where encapsulated complexes are evidently appeared to be much more reactive for oxidative transformation than the corresponding free-state complex.[24, 38-43] Some other reports on the encapsulated metal phthalocyanine and Tris(2,2' bipyridine) iron complexes for the oxidation reaction for phenols, styrene, and methyl styrene also confirm that the free-state complex especially Tris(2,2′bipyridine) iron complex is definitely not so efficient catalyst like its encapsulated analogue under identical reaction conditions. A comparative study of different metal picolinato complexes in zeolite Y reported by R.C. Deka *et al.* has confirmed the encapsulated copper and cobalt complexes more reactive catalysts compared to the corresponding nickel complexes for the selective oxidation of phenol by using H_2O_2 as the oxidant.[7, 44, 45] Recently, R. Ananthakrishnan and coworkers have reported the synthesis of $[Ru(bpy)_3]Cl_2$ complex on a mesoporous silica SBA-15 support and its application for degradation of chlorophenol under visible light in an aqueous medium.[46] In another report, an encapsulated chiral nickel Schiff base complexes inside the cavity of zeolite Y has been recognized as an excellent catalyst for asymmetric Henry reaction.[47]

Copper complexes entrapped in the cavities of zeolites are recognized to show high catalytic activity in certain organic reactions. In general, there are many attempts to achieve the reactions with high yield and selectivity. Zeolite encapsulated copper(II) hexaazamacrocyclic complexes studied for the degradation of Reactive Red 198 and Phenol Red dyes. These reusable photocatalysts exhibit good catalytic efficiency for the degradation of dyes.[48] Copper complex of tetradentate N_2O_2 Schiff-base ligand is synthesized inside the zeolite-Y that is employed as catalyst for the oxidation of benzhydrol and degradation of rhodamine B dye. Upon encapsulation, this complex shows enhanced activity for both the reactions.[49] Catalytic oxidation of benzene, styrene, phenol and cyclohexene is carried out by using copper(II) Schiff-base complexes in homogenous and heterogeneous media.[50] Encapsulated complexes show enhanced selectivity and turnover frequency (TOF) values as compared to their free-state analogues.

It is quite clear that the encapsulated complexes in zeolite Y are competent catalysts for oxidation of hydrocarbons, and most of the studies have suggested that enhanced activity of the encapsulated complex

is definitely a consequence of the distorted geometry of the complex under space constraint inside the rigid cavity.[51, 52]Already, the diverse effects of different substituents on the structure and functionality of the copper Schiff-base complexes are discussed thoroughly.[53] Bhadbhade *et al.* have explored the effect of substituents (H, -OCH_3 and -Cl on Cu-salen, 5-OCH_3-Cu-salen, and 5-chloro-Cu-salen) on various aspects like molecular association, conformation, and electronic structure. Cu-salen complex forms strong dimers adopting stepped confirmation and 5-OCH_3-Cu-salen complex with an electron donating -OCH_3 substituent maintains more planarity around the metal center proximity and forms weak dimer. However, an electron-withdrawing chloro-substituted complex (5-chloro-Cu-salen) is essentially a monomer in solid state and has distorted square-planar geometry around CuN_2O_2 proximity.[53] It is interesting to observe the diverse effects of molecular association e.g., steric and electronic effects and ligand architecture on the reactivity of the catalyst in the homogeneous and heterogeneous states.

In the present study, we choose the complexes with different substitution (H, OH, Br and - OCH_3 on the 5^{th} position of the phenyl rings) of Schiff base salophen ligands. These copper salophen complexes are abbreviated as CuL1, CuL2, CuL3 and CuL5. In this series, the molecular dimension of the complexes follows the increasing order from CuL1 to CuL5and these are encapsulated inside nearly spherical supercage of zeolite Y via flexible ligand synthesis method (given in Figure 3.1). These systems are well characterized with the help of powdered XRD, AAS, SEM-EDS, IR, XPS, TGA, BET and UV-Visible spectroscopy. These systems are employed as catalysts for the styrene oxidation reaction.

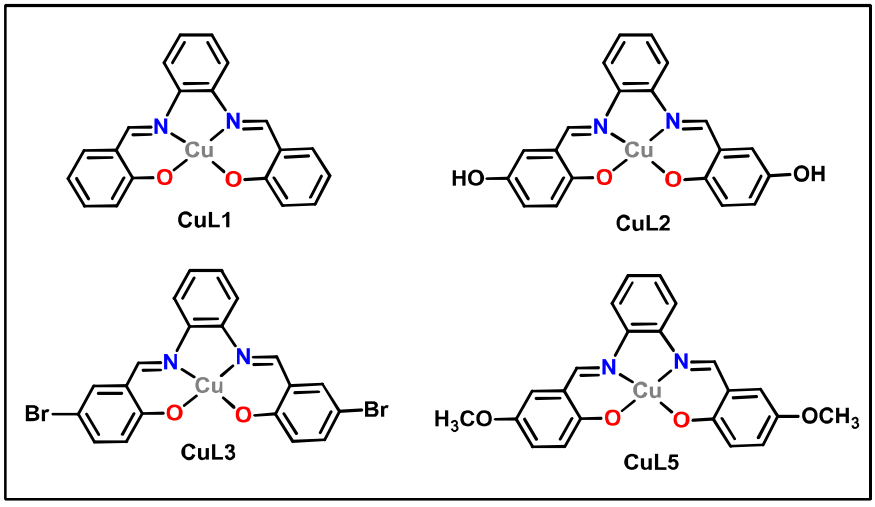

Figure 3.1: Schematic representation of copper Schiff-base complexes.

The encapsulation and catalysis of different copper complexes in the voids of zeolite Y are extensively studied[24, 49, 54-57]; however, there is scarcity of systematic approach to study the structural changes of the complexes upon encapsulation. Research to associate the enhanced selective catalysis and adopted geometry of the guest complex is relatively rare in the literature and our research attempts to address this question. The selection of the copper Schiff-base complexes largely depends upon the end-to-end distance of the complex so that the host supercage of 12.47 Å diameter imposes the steric constraints on the guest complex. Under such condition, the geometry adopted by the complex are studied thoroughly. Detailed studies of modified reactivity towards styrene oxidation evolving from structural distortion, as a function of the end-to-end distance of the complex is the prime objective of our research.

Comparative structural and catalytic studies of these coupled systems have been carried out in detail to comprehend the geometry of the complex after encapsulation as well as to identify the origin of the modified functionality of the systems. Associate the enhanced selective catalysis and adopted geometry of the guest complex is relatively rare in the literature and our research attempts to address this question. Comparative studies reveal quite a fascinating correlation existing between the catalytic activities and modified structure experienced by the complexes under encapsulation, which leaves a lot of scopes to further modify the activity of the catalysts and to have a better insight of these heterogeneous systems.

3.2 RESULTS AND DISCUSSION

Detailed Synthesis of ligands and copper Schiff-base complexes in free or encapsulated states have already been discussed in chapter 2 under experimental section (2.2.1-2.2.5).

3.2.1 Elemental Analysis

Parent zeolite has Si/Al ratio of 2.34 and its unit cell formula of the host material is $Na_{58}Al_{58}Si_{136}O_{388}$ yH_2O. The Si/Al ratio of host framework remains unaffected even after the complete synthesis of the metal complex inside it, which essentially signifies the lack of dealumination during the whole process of ion exchange and encapsulation.[58] The concentration of metals in different samples are determined by atomic absorption spectroscopy (AAS) and it is found that the metal content in the encapsulated Cu complexes is always less than that present in the Cu- exchanged zeolite Y (AAS data given in Table 3.6). The observation essentially indicates the complex formation inside the host cavity with slight leaching of some of the metal ions during the process of encapsulation.

3.2.2 X-Ray Diffraction and Scanning Electron Microscopy Analysis

To investigate the order of retention of zeolite crystallinity, surface morphology, and integrity of host zeolite Y, XRD patterns of parent zeolite Y, Cu-zeolite Y and zeolite with encapsulated copper Schiff-base complexes are recorded. (XRD pattern are given in Figure 3.2) Essentially similar patterns of all the samples indicate the preservation of the integrity of the host framework during the process of encapsulation. On comparison of the XRD patterns of encapsulated complexes with the pure and copper exchanged zeolite-Y, an evident distinction in the XRD patterns of the encapsulated complexes has been observed. Alteration of relative intensities of peaks at the $2\theta = 10°$ and $12°$ are noticed after encapsulation. For parent zeolite and Cu-exchanged zeolite, the relation $I_{220} > I_{311}$ exist, but for zeolite, with encapsulated complexes, the relation is just reverse; $I_{311} > I_{220}$. The observed modification in these intensities after the encapsulation previously has been recognized and empirically associated with the fact that a large complex is indeed present within the zeolite-Y supercage.[59]

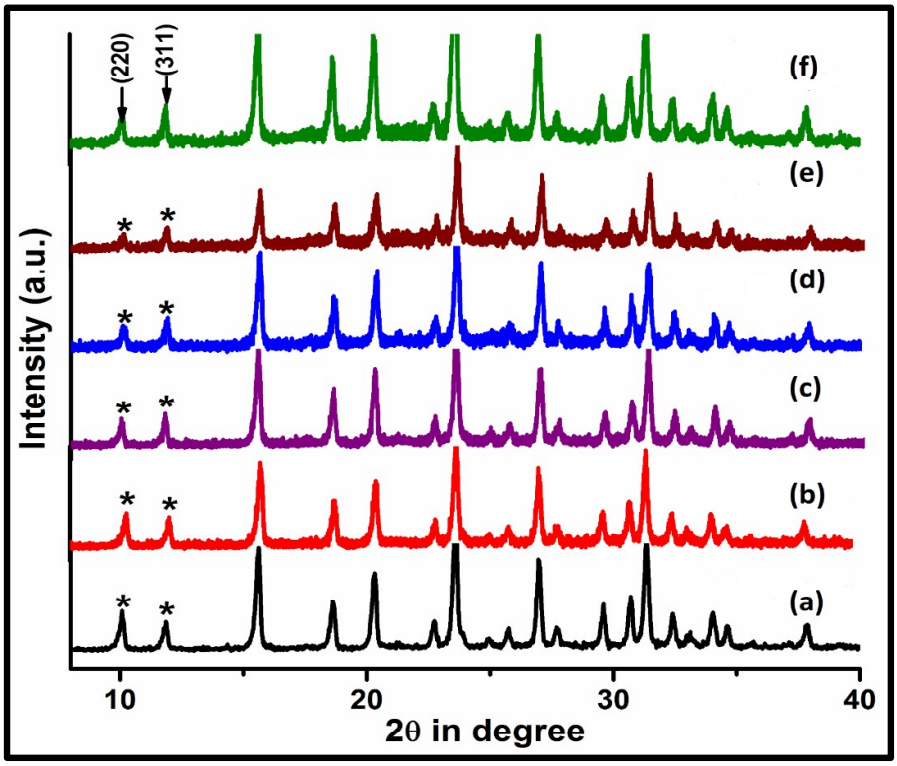

Figure 3.2: Powder XRD patterns of (a) pure zeolite-Y (b) Cu- exchanged zeolite-Y, (c) CuL1-Y, (d) CuL2-Y, (e) CuL3-Y and (f) CuL5-Y.

Scanning electron microscopy also supports the fact that the complex formation is primarily taking place inside the host cavities. From the SEM images (SEM micrographs given in Figure 3.3A-3.3C before Soxhlet extraction for CuL5-Y with different resolution and Figure 3.3D-3.3F for CuL5-Y after Soxhlet extraction. It is observed that before Soxhlet extraction, there are some detectable surface species probably due to the formation of the complex at the surface or un-reacted ligands; however, these are disappeared after Soxhlet extraction.[58, 60] The clarity in the observation of boundaries of host lattice in SEM micrographs and the persistent color of Soxhlet extracted final product are certainly logical indications of successful encapsulation of the complex inside the cavities of zeolite Y.

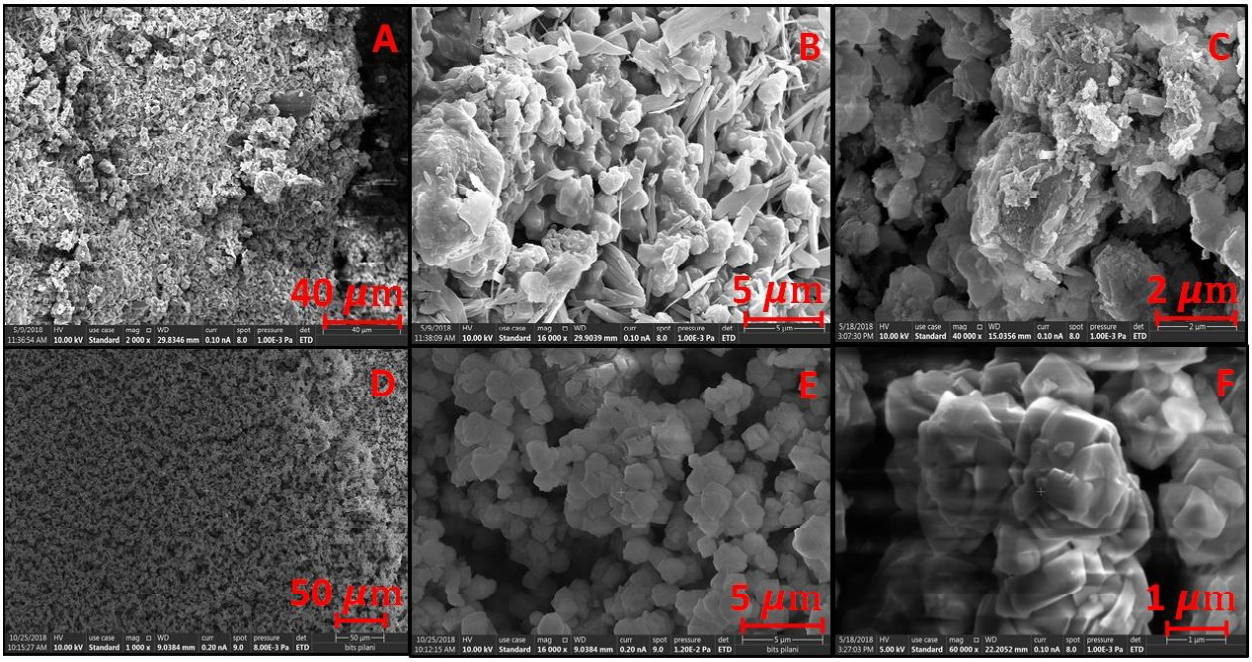

Figure 3.3: SEM images of CuL5-Y sample with different resolution; (A-C) before Soxhlet extraction, and (D-F) after Soxhlet extraction.

3.2.3 IR Spectroscopic study

IR spectral data of pure zeolite Y and all copper Schiff-base complexes in free and encapsulated states are given in Figure 3.4 and Table 3.1. Pure zeolite Y has shown strong IR peak at 1018 cm^{-1}, which is mainly attributed to the presence of asymmetric stretching vibrations of $(Si/Al)O_4$ units of the framework. Other some prominent peaks are present at 560, 717, 786, 1643 and 3500 cm^{-1} position, which are mainly

assigned to $(Si/Al)O_4$ bending mode, double ring, symmetric stretching vibrations, other two IR bands at 1643 and 3500 cm^{-1} positions are attributed to lattice water molecules and surface hydroxylic group.[7, 60] These IR bands are remaining unaffected even after encapsulation processes. All the encapsulated complexes have exhibited the bands without any significant alternation in the peak positions, evidently revealing the fact that the host framework is not modified during the complex formation inside the supercage. The suitable IR region for the characterization of encapsulated Schiff-base complex is 1200-1600 cm^{-1}, because in this region host lattice remains silent and observed IR peaks with smaller shifts are mainly due to the presence of guest complex within the framework having different environment from its free state. Studies in this region of 1200-1600 cm^{-1} become beneficial as some of the significant IR bands of the Schiff base complexes like C=N, C=C, C-O stretching and C-H deformation have emerged in this particular region, which are unaffected by host lattice. Comparative IR data indicates the complex formation in neat as well as in encapsulated state. In the encapsulated complexes, C=N and C-O stretching bands appear at comparative positions to free state complex and the higher shifts in ν_{C-H} deformation frequencies have already been attributed to the presence of complex inside the zeolite cavity[61]. The observed FTIR spectral data (Table 3.1) suggest the formation of copper Schiff-base complexes in the free and encapsulated states inside the zeolite Y supercage.

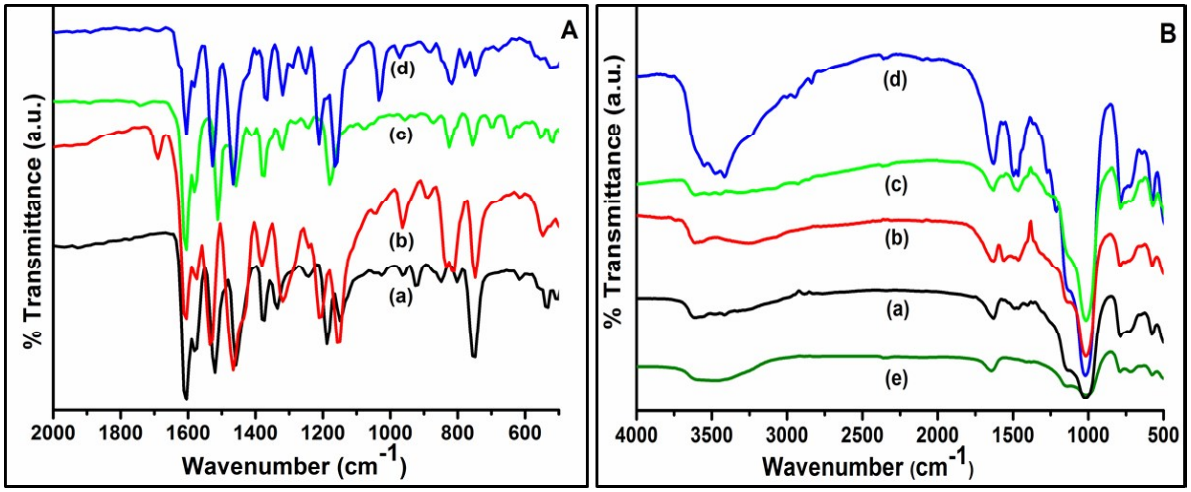

Figure 3.4: (A) FTIR spectra of free-state copper salophen complexes (a) CuL1, (b) CuL2, (c) CuL3 and (d) CuL5. (B) FTIR spectra of encapsulated copper salophen complexes (a) CuL1-Y, (b) CuL2-Y, (c) CuL3-Y, (d) CuL5-Y and (e) pure zeolite-Y.

Table 3.1: FTIR spectral data (in cm^{-1}) for neat and encapsulated state complexes.

S. No	Samples	C=N stretching	C=C stretching	C-H deformation	C-O stretching
1	CuL1	1606	1520, 1458	1373	1242
2	CuL1-Y	1628	1489, 1466	1366	1240
3	CuL2	1605	1542, 1466	1381	1211
4	CuL2-Y	1628	1558, 1466	1382	1215
5	CuL3	1605	1512, 1458	1373	1242
6	CuL3-Y	1628	1566, 1466	1392	1239
7	CuL5	1605	1528, 1466	1366	1211
8	CuL5-Y	1628	1466	1382	1212

3.2.4 X-Ray Photoelectron Spectroscopy (XPS)

The existence of the guest metal complex in zeolite Y is also confirmed with the help of XPS study, which is an indirect technique to investigate the location of the metal complex in the host framework. The XPS survey spectra (given in Figure 3.5) and binding energy data of CuL1 and CuL1-Y are presented in Table 3.2. It is observed that the elements/metal ions (C, N, O, Si, Al, and Cu^{2+}) are present in their respective surface chemical states in these complexes. The low concentration of metal contents in the encapsulated systems results the XPS signal weak for metal, which is actually in accordance with the concentration-dependent studies like IR, UV-Vis spectroscopy. The appearance of Cu(2p) peaks in XPS spectrum confirms the presence of copper and is assigned to the Cu $2p_{3/2}$ and Cu $2p_{1/2}$ confirms the +2 oxidation state of Cu and square planar geometry of the complexes in the free and encapsulated states. Cu $2p_{3/2}$ and Cu $2p_{1/2}$ XPS signals have appeared at the binding energies of 932.80 eV and 952.72 eV respectively for the CuL1 complex, whereas for the encapsulated complex (CuL1-Y) these peaks are slightly shifted towards the higher binding energies and have appeared at 934.17 and 954.13eV respectively.[7, 62] (XPS spectra presented in Figure 3.6) Such observed higher shifts in the binding energies upon encapsulation

could be the result of lowering of electron density on the metal center because of the weakening in the delocalization of electrons due to alteration in the square planar proximity of the encapsulated complex.[7] However, XPS signals for other atoms are more or less unshifted. For CuL1 complex, the C(1s) XPS signals are observed at 283.35, 285.03 eV and attributed to sp^2, sp^3 carbon atom whereas signals at 397.68, 399.61 eV and 531.26, 533.74 eV are attributed to (M-N, C=N) and (M-O, C-O) form of the respective elements (XPS spectra are presented in Figure 3.7). These XPS peaks are observed at almost identical binding energies for the encapsulated complex. For CuL1-Y-complex, C (1s) appear at 284.13 and 285.41 eV, which corresponds to the sp^2 and sp^3 carbon atoms respectively.[62] N (1s) peaks for the complex are observed at binding energies 399.18 eV (M-N) and 401.65 eV (C=N) whereas O (1s) peaks appear at the binding energies of 530.66 eV (M-O) and 532.88 eV (C-O).[51, 62] Furthermore, the encapsulated copper complex has shown zeolitic Na(1s), Al(2p) and Si(2p) XPS signals at their respective positions[7, 51, 62](XPS spectra are shown in Figure 3.8). Comparative XPS binding energy data of both free and encapsulated complex, as well as higher shifts in binding energy for the Cu $2p_{3/2}$ and Cu $2p_{1/2}$ peaks in case of encapsulated copper complex, essentially signify the encapsulation of metal complexes inside the zeolite Y.

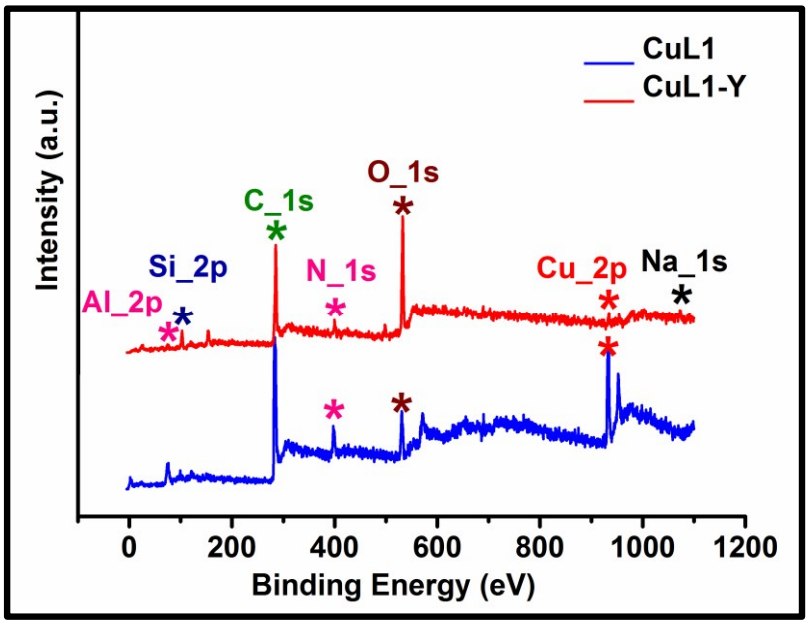

Figure 3.5: XPS survey spectra of (a) CuL1 and (b) CuL1-Y.

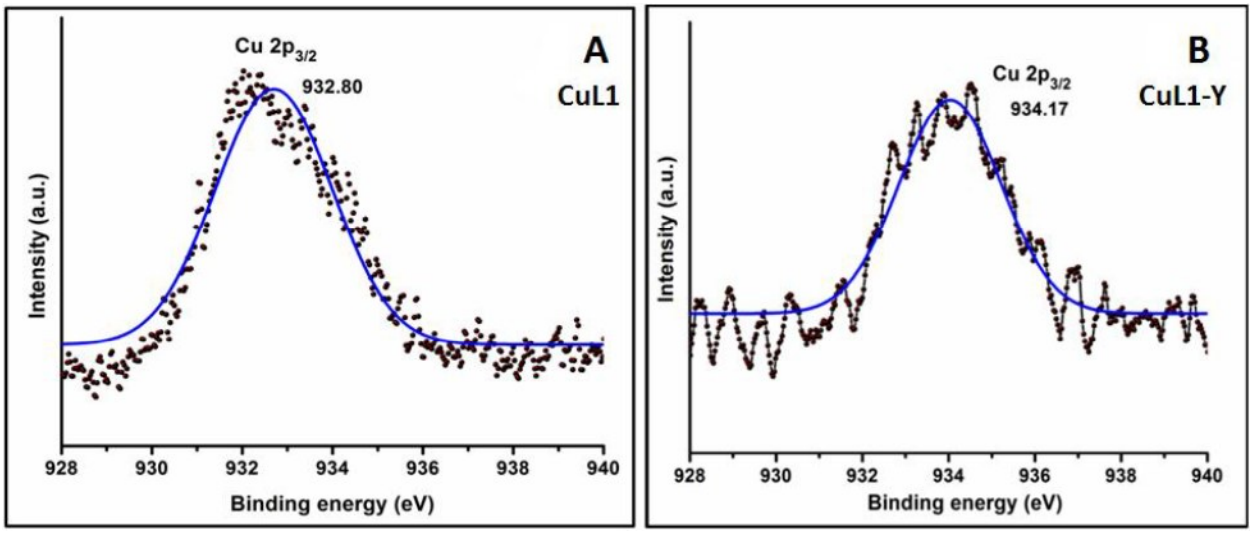

Figure 3.6: High-resolution XPS spectra for the Cu $2p_{3/2}$ signal (A) CuL1 and (B) CuL1- Y.

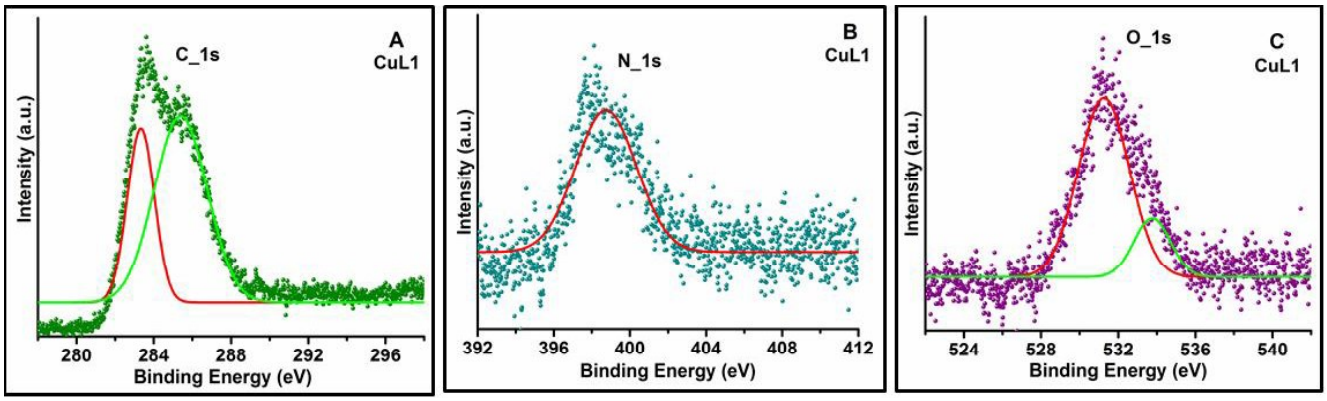

Figure 3.7: High-resolution peak fitted XPS spectra of (A) C (1s), (B) N (1s) and (C) O (1s) for CuL1.

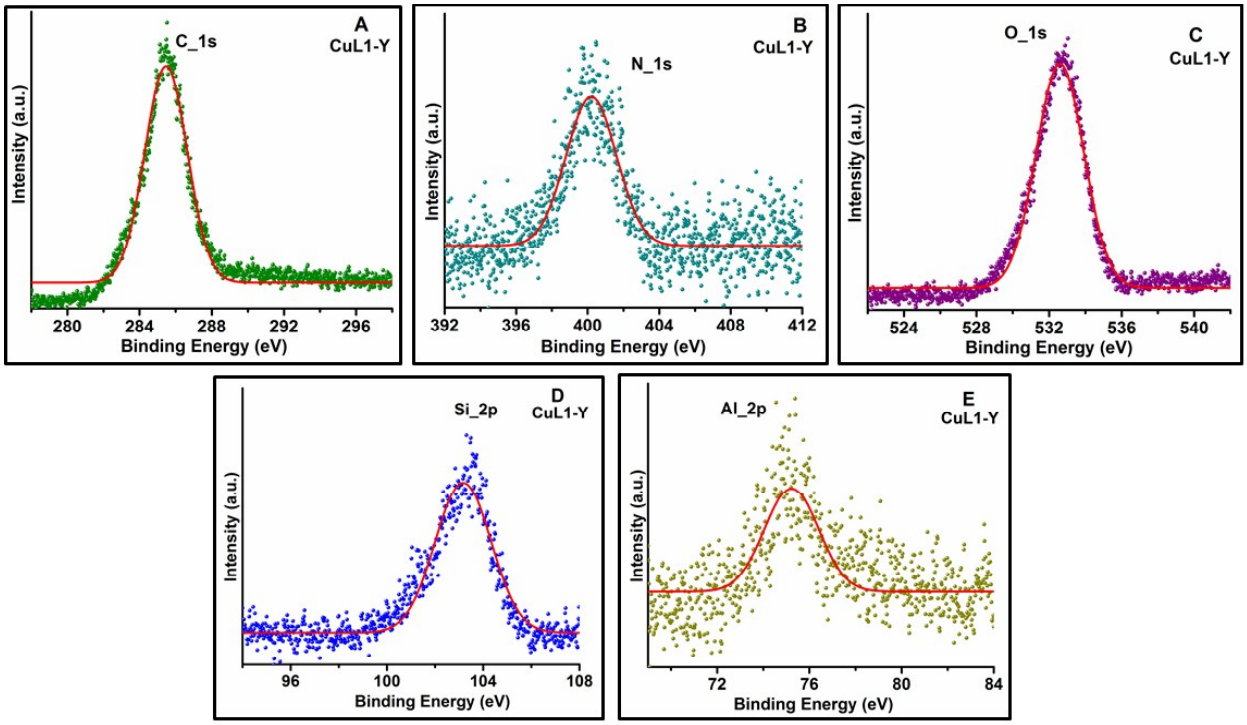

Figure 3.8: High-resolution XPS spectra of (A) C (1s), (B) N (1s), (C) O (1s), (D) Si (2p) and (E) Al (2p) for CuL1-Y.

Table 3.2: Binding energy (eV) of free and encapsulated complexes.

S. No	Samples	Binding energy (eV)						
		Si (2p)	Al (2p)	C (1s)	N (1s)	O (1s)	Cu^{2+} (2p)	Δ2p
1	CuL1	-	-	283.35, 285.03	397.68, 399.61	531.26, 533.74	932.80, 952.72	19.92
2	CuL1-Y	103.56	75.23	284.13, 285.41	399.18 401.65	530.66, 532.88	934.17, 954.13	19.96

3.2.5 Thermogravimetric Analysis (TGA)

The TGA curves of pure zeolite Y, neat and encapsulated complexes are obtained in a nitrogen atmosphere and are shown in Figure 3.9 (TGA data are given in Table 3.3). According to the TGA curve, weight loss for the neat copper complex CuL5 occurred in two steps. The first weight loss takes place in the temperature range (308-360)℃ and in the second step, weight loss starts immediately after the first step in the range (361-575)℃ suggesting decomposition of the chelating salophen ligand.[47] For pure zeolite Y, weight loss (24%) is obtained in the one-step temperature range of (50-300)℃ due to the loss of intrazeolite water molecules.[63] Unlike pure zeolite Y, the encapsulated copper salophen complex CuL5-Y shows two-step weight losses. The first step weight loss occurs in the range of (50-300)℃ corresponding to desorption of physically adsorbed water molecules from the zeolite framework with a mass loss of 11.3%. The second step involves the weight loss occurring after 320℃ with a mass loss of 31.1% which definitely corresponds to the loss of organic moieties from the zeolite cages.[63]

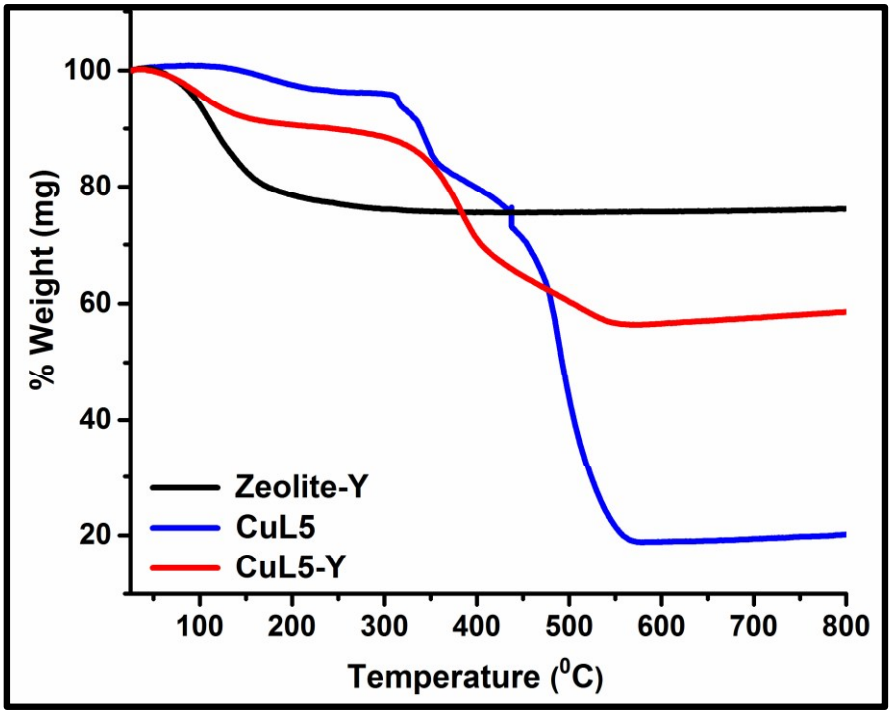

Figure 3.9: TGA curves of pure zeolite-Y, CuL5 and CuL5-Y.

Table 3.3: Thermogravimetric analysis data of free and encapsulated complexes.

S.No.	Samples	Temperature range (°C)	Weight loss (%)
1	**Zeolite-Y**	50-300	24.0
2	**CuL5**	308-360	13.0
		361-575	64.8
3	**CuL5-Y**	50-300	11.3
		320-580	31.1

3.2.6 BET surface area analysis

The BET surface area analysis has been performed to find out the surface area and pore volume of pure zeolite Y and encapsulated complexes. The comparative N_2 adsorption-desorption isotherms for zeolite Y and encapsulated copper complex (CuL5-Y) using BJH method are shown in Figure 3.10 along with the data of surface area and micropore volume, given in Table 3.4. The pattern of nitrogen sorption isotherms for both the samples are found to be nearly identical (Figure 3.10), indicating that the zeolite framework is not affected during the encapsulation process. Both the samples have shown type I adsorption-desorption isotherms, which is a characteristic of the microporous material.[64] The lowering of BET surface areas and pore volumes of the zeolite sample with encapsulated copper complex compared to that of pure zeolite Y clearly suggest the presence of metal complex within the supercage of zeolite Y rather than on the external surface.[43, 47] The decreases in the surface area and pore volume of the catalyst largely depend upon the loading level of metal in zeolites along with the molecular dimension and geometry of the complex encapsulated inside the zeolite supercage.

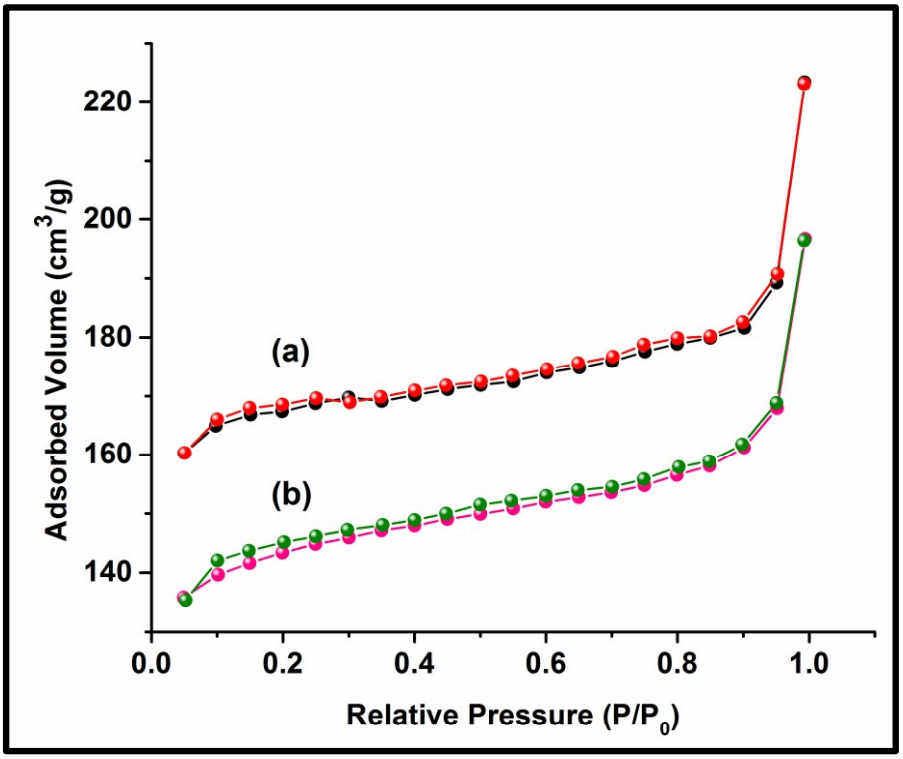

Figure 3.10: BET isotherms for pure zeolite-Y and zeolite encapsulated complexes: (a) pure zeolite Y and (b) CuL5-Y.

Table 3.4: BET surface area and pore volume of pure zeolite Y and encapsulated complex CuL5-Y.

S.No.	Sample	BET surface area (m^2/g)	Pore volume (cm^3/g)
1	**Pure zeolite Y**	535	0.3456
2	**CuL5-Y**	420	0.2611

3.2.7 UV-Visible Study

To confirm the complex formation inside the cavity of zeolite and to study the coordination environment around the metal center, electronic spectroscopy is always being informative. The relative UV-Visible

spectroscopic studies in the solid-state of all the copper Schiff-base complexes presented in Figure 3.11 and Table 3.5.

Absorption bands in the range of (230-250) nm are recognized as π-π* transitions, whereas in the range of (300-384) nm are mainly assigned as n-π* transitions. The electronic transitions, which are mainly originated from the metal d orbitals, are identified in the comparative lower energy region of the spectrum. Bands appeared in the range of (404-471) nm and (502-607) nm are attributed to charge transfer and d-d transitions respectively. UV-Visible data of free CuL1 complex have shown good concurrence with the reported data in the literature[65] and also provided the information about the complex formation in the free state. After the encapsulation in zeolite Y, complexes have shown a similar prototype of electronic spectra, indicating that the complexes are indeed present in the host lattice. Comparative studies of the electronic spectra of the complexes in free and their encapsulated states, make it quite clear that the intra-ligand transitions (π-π* and n-π*) are relatively unaffected under the encapsulation; however, transitions which are mainly instigated from the metal center are primarily altered in terms of peak positions as well as intensities for all guest complexes. It is quite interesting to perceive a regular blue shift and intensification of the d-d transitions in the encapsulated copper - Schiff-base complexes. Such behavior already has been observed in the zeolite Y encapsulated complexes.[51, 58, 61] Observed modified electronic behavior in the d-d region is certainly an effect of different geometry of the coordination sphere, which the guest complex has adopted under the space restrictions of host supercage. Theoretical studies have also revealed the fact that changes in the bond angles, bond lengths, and HOMO-LUMO gaps can be introduced in the guest complex by the process of encapsulation in zeolites.[58, 60] In the present study, the copper complexes have chosen based on their molecular dimensions (i.e., end to end distances) of the complexes, which follow the order as CuL1 <CuL2 <CuL3 <CuL5 for the salophen copper complexes. The complex with larger molecular dimensions experiences the more steric impulsion and obviously, it adopts more distorted geometry to accommodate itself into the framework cavity. There are some interesting reports, which have explored the correlation between the geometry of the metal complexes and different factors and their consequence. It is previously studied that effect of the substituent groups (-Cl and $–OCH_3$) on the geometry of copper Schiff-base complexes is very prominent.[2, 66] Another report has revealed that the replacement of the atoms in the N_2O_2 square planar proximity by N_2OS and N_2S_2 leads the distortion in the geometry of that complex and resultant effect can be seen in the optical behavior of that complex.[67] Sankar *et al.*

have suggested that the different substituent groups can cause the push-pull effect on the porphyrin complexes which is associated with the change in the energy gaps in the d-d orbitals.[68] In the current study, we have observed a nice correlation between the observed blue shift in d-d bands and the molecular dimensions of the copper Schiff base complexes. On encapsulation, the complex with largest molecular dimension CuL5-Y is expected to adopt the most distorted geometry, which is actually depicted as maximum blue-shifted d-d band in the electronic spectrum, whereas CuL1 complex has shown minimum blue shift. The degree of blue shift in d-d band is just in accordance to the increasing order of the molecular dimensions of complexes and the order is CuL1<CuL2<CuL3<CuL5 for the salophen complexes. This behavior of complexes is quite reasonable and can be well-correlated with the extent of distortion and molecular dimensions of the guest complex and their consequence in the optical spectra.

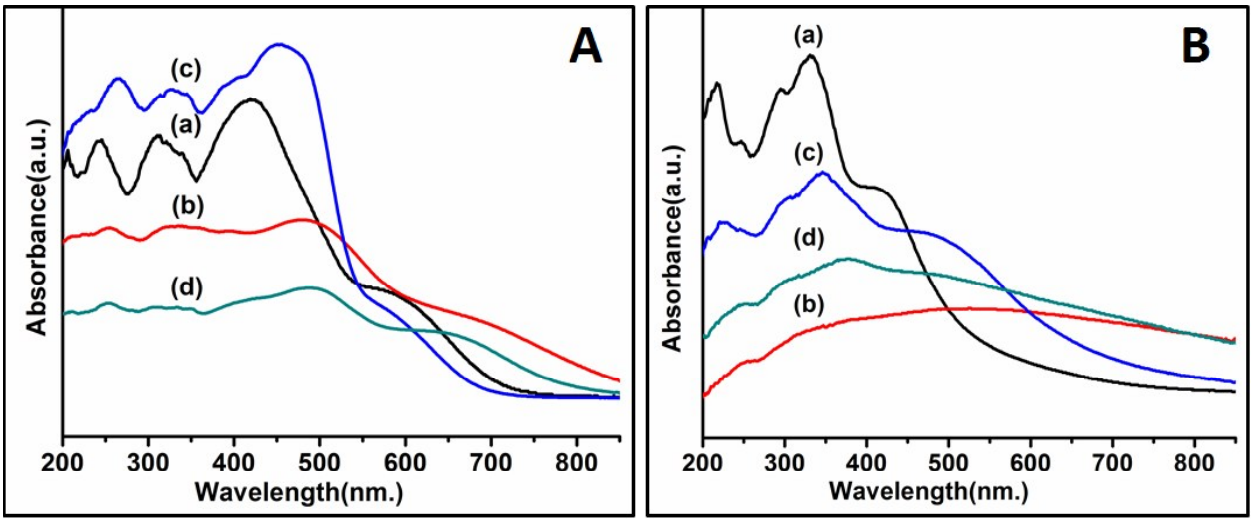

Figure 3.11: (A) The solid-state UV-Vis spectra of copper salophen complexes (a) CuL1, (b) CuL2, (c) CuL3 and (d) CuL5. (B) The solid-state UV-Vis spectra of encapsulated copper salophen complexes in zeolite Y (a) CuL1-Y, (b) CuL2-Y, (c) CuL3-Y and (d) CuL5-Y.

Table 3.5: Solid-state UV-Visible spectroscopic data of complexes in free and encapsulated state.

S.No	Samples	π—π^* transitions	n—π^* transitions	CT transitions	d-d transitions
1	**CuL1**	246	306	419	607
2	**CuL1-Y**	249	300	423	588
3	**CuL2**	251	347	479	668
4	**CuL2-Y**	253	343	394	567
5	**CuL3**	249	336	445	502
6	**CuL3-Y**	247	338	471	610
7	**CuL5**	253	321	484	646
8	**CuL5-Y**	251	315	382	503

3.2.8 Catalytic Study

Catalytic activities of the metal complexes in their free state as well as encapsulated states are explored for the oxidation of styrene and then compared. Styrene can be oxidized into the different organic compounds as benzaldehyde, styrene oxide, benzoic acid, phenylacetaldehyde and phenylethane-1, 2-diol; some of these products of the reaction are previously reported.[24, 38] Calibration curve of styrene, benzaldehyde and styrene oxide are shown in Figure 3.12. Reaction conditions are optimized with respect to the encapsulated copper complex as catalyst by varying different reaction parameters like temperature, the time duration of reaction and amount of catalysts to attain maximum efficiency. To standardize the reaction condition, styrene (1.56 g, 15 mmol) and 30% H_2O_2 (3.40 g, 30 mmol) are mixed with 15 ml acetonitrile and catalysts of different amounts (0.015 g, 0.030 g and 0.05 g) are added at various temperatures 40℃, 80℃ and 120℃ for variable reaction durations (2 h, 5 h and 8 h). Initially, the amount of catalyst is optimized, as it has shown the improved reactivity when employed in two different sets of reaction with 0.030 g and 0.050 g. The conversion of styrene is found to be the least when 0.015g of the catalyst is used (catalytic data are presented in Figure 3.13). We have considered 0.050 g as an optimized

amount of the catalysts for above reaction conditions because no substantial improvement in the % conversion of styrene is observed while taking 0.070 g of the catalysts. A further increase in the amount of catalyst causes a drop in % conversion since it lowers the probably of adsorption of two different reactant molecules on the same catalytic site hence reduces the effective interaction between reactant molecules.[38]

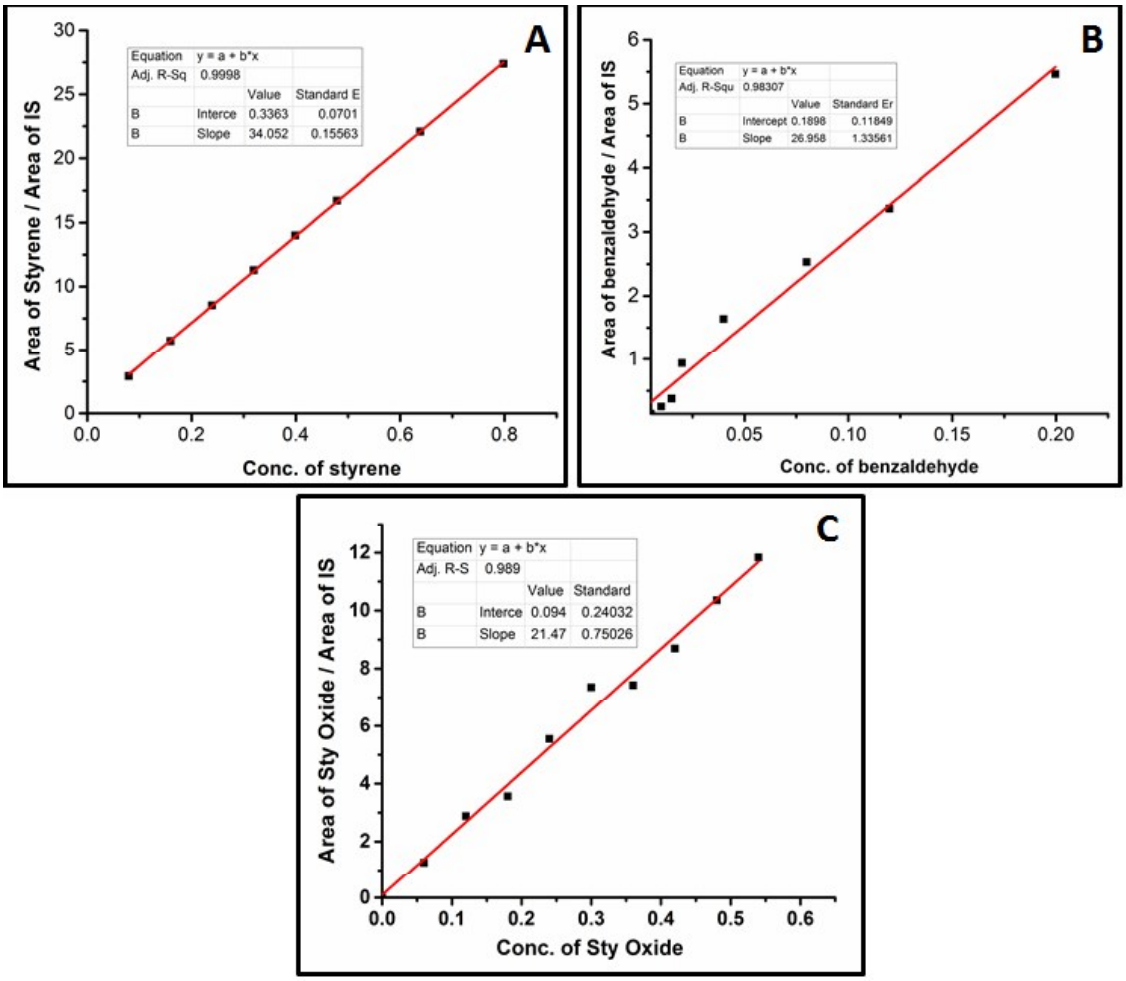

Figure 3.12: Calibration curve of (A) styrene, (B) benzaldehyde and (C) styrene oxide.

For the oxidation reaction, styrene (1.56 g, 15 mmol), 30% H_2O_2 (3.40 g, 30 mmol) in 15 ml acetonitrile and 0.050 g catalyst have been kept for different time durations e.g., 2 h, 5 h and 8 h. Since there is no significant improvement observed in the % conversion of styrene after 8 h and this is chosen as the adequate time for the reaction. With these optimized conditions, the styrene oxidation reaction is studied

at three different temperatures 40℃, 80℃ and 120℃, and conversion of styrene is quantified as 5%, 47% and 58% for the encapsulated copper complex at 40℃, 80℃ and 120℃ respectively. Therefore, 80℃ temperature is found to be the appropriate/optimum temperature for the reaction. However, for the free state complexes, quite a low amount of 0.0045 g has been employed as a catalyst in each of the cases because concentration of active metal centers in neat complexes is much higher i.e., much more in number as compared to their analogous encapsulated state complexes. Comparative studies (shown in Table 3.6) clearly indicate that 0.0045 g free state complex still contains 2-4 times higher the number of Cu active centers than that present in 0.05 g of the corresponding encapsulated complex. Within the optimum range of the amount of catalyst, more the number of active metal sites more is the % conversion of styrene. Therefore, to study catalysis driven by the geometry of the metal complex, the rationale is to present the catalytic information in terms of the turnover number (TON) rather than the % conversion so that difference in concentrations of active metal centers in both the states could be nullified. With these suitable conditions, copper salophen complexes (CuL1, CuL2, CuL3, and CuL5) are employed as catalysts in free as well as encapsulated states (catalytic data presented in Table 3.7). These catalysts are more selective for benzaldehyde formation in both states, while the other products like styrene oxide are formed as a minor product along with negligibly small amounts of benzoic acid and phenylacetaldehyde. The higher yield of benzaldehyde might be associated with the formation of hydroperoxylstyrene intermediate by the nucleophilic attack of H_2O_2, which is further cleaved to produce benzaldehyde. Another route of formation of benzaldehyde is further oxidation of styrene oxide, one of the products of the styrene oxidation. The formation of benzoic acid is the result of further oxidation of benzaldehyde and phenylacetaldehyde is the isomerized product of styrene oxide.[69]

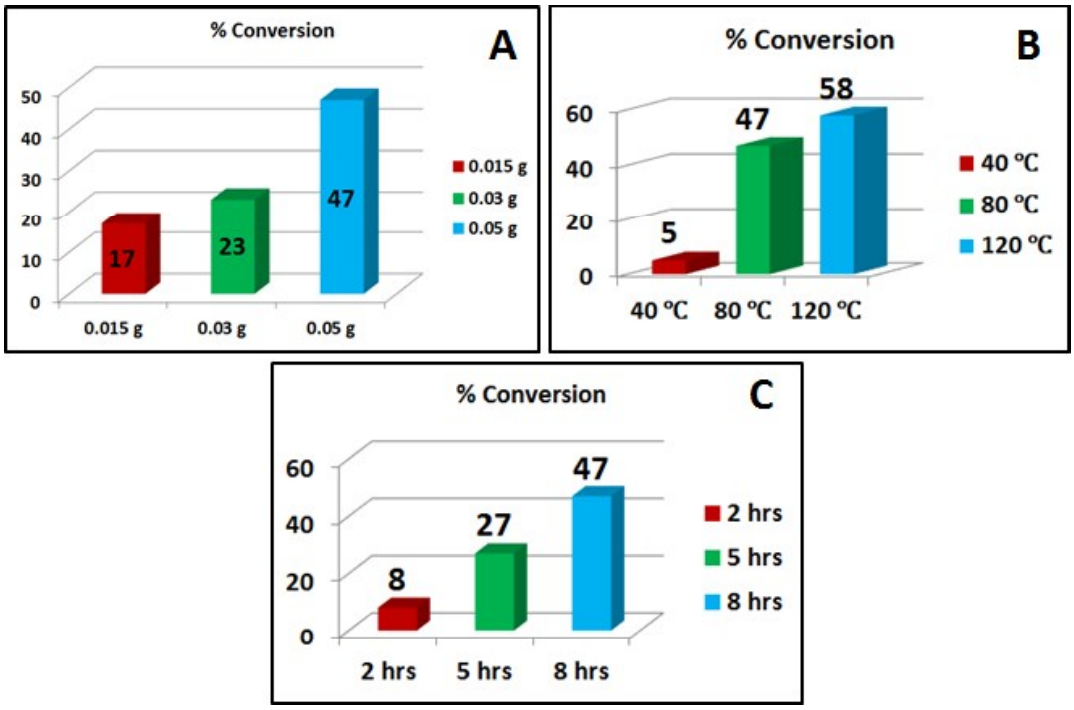

Figure 3.13: % Conversion of styrene for encapsulated copper complex with respect to (A) amount of catalyst, (B) temperature of reaction and (C) different time duration.

Table 3.6: Amount of Cu-atom (mmol) for all catalysts.

S. No	Catalyst	Cu-atom in catalyst (mmol)[a]	S. No	Catalyst	% weight of Cu[b]	Cu-atom in catalyst (mmol) [a]
1	**Zeolite-Y**	-	**2**	**Cu-Y**	0.81	0.00637
3	**CuL1**	0.01190	**4**	**CuL1-Y**	0.67	0.00527
5	**CuL2**	0.01090	**6**	**CuL2-Y**	0.52	0.00409
7	**CuL3**	0.00840	**8**	**CuL3-Y**	0.39	0.00306
9	**CuL5**	0.01020	**10**	**CuL5-Y**	0.34	0.00267

[a] mmol of Cu atom calculated in 0.0045 g for neat complexes and 0.05 g for encapsulated complexes and Cu-Y.

[b] % weight of Cu obtained from AAS.

Turn over number (TON) calculated from the catalytic data have repeatedly shown a clear-cut reactivity trend; free state copper salophen complexes follow the reactivity order as CuL1 >CuL3 >CuL2 >CuL5 however upon encapsulation within zeolite Y, scenario changes. The encapsulated salophen complexes demonstrate the order as CuL5 >CuL3 >CuL2 >CuL1. The catalytic activity is certainly governed by the electronic factor or electron density on the metal when the complexes are in their free states.

Table 3.7: Conversion of styrene after 8 h reaction time with H_2O_2 as oxidant.

S. No	Samples	% Conversion	TON	Selectivity	
				Benz.	SO
1	**Zeolite-Y**	3	-	73.97	26.02
2	**Cu-Y**	20	455.2	90.90	9.09
3	**CuL1**	74	937.8	89.47	10.52
4	**CuL1-Y**	50	1423.1	93.15	6.84
5	**CuL2**	59	807.3	89.62	10.37
6	**CuL2-Y**	57	2078.2	91.05	8.94
7	**CuL3**	50	892.8	95.45	4.54
8	**CuL3-Y**	62	3042.4	97.56	2.43
9	**CuL5**	12	187.2	93.41	6.59
10	**CuL5-Y**	63	3543	95.17	4.82

Reaction conditions: Styrene: 1.56 g (15 mmol), H_2O_2: 3.40 g (30 mmol), acetonitrile 15 ml, temperature 80°C, catalyst (0.05 g for encapsulated complexes and 0.0045 g for neat complexes), TON (turn over number): mole of substrate converted per mole of metal center, Benz.: Benzaldehyde, SO: Styrene oxide.

Complexes with different substituent groups render electron density of the metal differently, and consequently, the outcome of catalysis varies. However, after encapsulation, the steric constraint imposed by the zeolite framework upon the guest complex contributes significantly to the catalytic activity. On

encapsulation, the complexes with larger molecular dimension possibly undergo more distortion imposed by the supercage, finally leading to the alteration of the overall reactivity order. Hence, the final structure adopted by the encapsulated complex is the major decisive factor for improved catalysis. Therefore, to understand or to verify the mechanism of a catalytic process with respect to the appropriate structural involvement of the catalyst, encapsulation could be a technically potent process. Detailed structural analysis of the complex especially after encapsulation inside zeolite is expected to provide the insight of the catalytic process hence, which indeed leads towards the tunable catalysis. The CuL5-Y catalyst is found to be efficient enough for this oxidation reaction up to six cycles with a marginal loss in its catalytic activity as in form of percentage conversion from 63% to 62.3% (Shown in Figure 3.14).

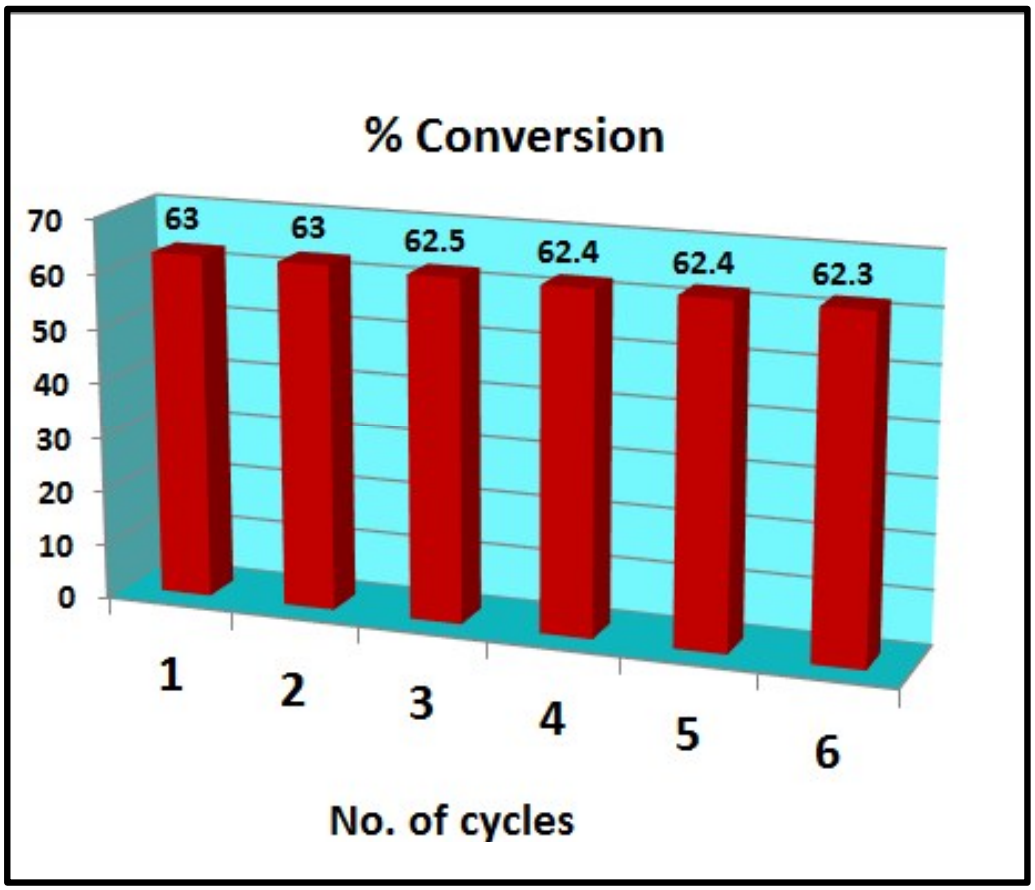

Figure 3.14: Recyclability of CuL5-Y catalyst for the styrene oxidation reaction.

The direct comparison of catalytic results presented in this work with literature data is not very straight-forward as the measuring parameters could be many. The results and the conditions from these studies are

summarized in table 3.8. In terms of the parameters like % conversion, product selectivity and TON, the catalyst of interest currently mentioned CuL5-Y competes well with other such catalysts.

Table 3.8: Comparison of catalysts performances for the oxidation of styrene

S.No.	Catalyst	Conversion (%)	Selectivity (%)		TON	Ref.
			Benz.	SO		
1	**Cu{salnptn(3-OMe)$_2$}**	97	68.6	31.3	303	[70]
2	**[CuCl(L^1)]-Y**	17.5	90.3	9.6	27.8	[71]
3	**[Cu(pydx-en)]-Y**	33.3	86.8	13.1	1074	[72]
4	**[Cu(pydx-1,3-pn)]-Y**	37.4	83.4	16.5	1290	[72]
5	**CuL5-Y**	**63**	**95.1**	**4.8**	**3543**	**This work**

3.2.9 Structural and functional Correlations

It is rather interesting to note that the reactivity in terms of turn over number (TON) of encapsulated complexes is substantially higher compared to the corresponding free state complexes. These observations signify that encapsulation within the supercage of zeolite has converted the metal complexes significantly reactive and hence, to achieve the same extent of activity, required active catalytic sites are much lesser in quantity. This makes the zeolite-encapsulated complexes as attractive heterogeneous catalysts for various organic oxidative transformations.[60, 69] The modified reactivity of the encapsulated complexes is mostly a consequence of the distorted geometry of the complexes they adopt, under encapsulation in zeolite Y. Copper Schiff-base complexes are generally efficient catalysts in solution as well as heterogeneous phases in comparisons to their corresponding nickel analogues. Crystal study of these complexes evidently indicates that copper metal is out of the square CuN_2O_2 proximity and shows distorted square planar geometry, whereas nickel Schiff base complexes are slightly less distorted retaining its nearly square planar geometry.[73]These complexes when encapsulated in zeolite Y, are further distorted due to space constraint imposed by rigid host zeolite supercage. Consequently, depletion in the electron density on the metal center takes place. Comparative shifts towards the higher value of binding energy in XPS signals for the zeolite-encapsulated complexes also support the generation of the more

electropositive metal center in encapsulated complexes. Encapsulation, therefore, appears to be an effective alternative approach to generate more electron-deficient metal center in a guest complex inside the rigid zeolite host.[2] Lower the electron density on the metal center, more receptive the metal center is for the nucleophilic attack. However, the depletion of electron density can also be achieved by addition of an electron withdrawing group (-Cl).[74] It has also been discussed that an electron-withdrawing (-Cl) substituent makes the complex essentially monomer in the solid state with distorted square-planar geometry around the metal. The report states that distorted chloro - copper salen complex provides the admixing of the ground state d_{xy} orbital with d_z^2 orbital and thereby enhances the stability of electron-rich axial ligand complex suggesting that electron-withdrawing group on the phenyl rings makes the metal complex significantly non-planar. However, an electron-donating group (-OCH_3) on the same position maintains the planarity of the complex. The planar conjugated system makes the metal center rich with electron density so that it acts as a less efficient receptive center for the nucleophilic attacks. Recently, it is observed experimentally as well as theoretically that the nickel (II) Schiff-base complexes with different molecular dimensions adopt distorted geometry under encapsulation in zeolite Y. The largest complex experiences more distortion and shows the most enhanced catalytic activity for styrene oxidation after the encapsulation. Interestingly, this complex is least reactive for the same catalytic process in its free state.[51] In the present study, the parallel behavior of zeolite Y encapsulated copper salophen complexes is observed for the oxidation of styrene in the presence of H_2O_2. Detailed catalytic studies for the series of copper Schiff-base complexes have indicated that electron-withdrawing –Br group present in the copper complex makes the complex distorted even in its free state (shown in Figure 3.16). Therefore, the complex is more reactive towards the nucleophillic attack stabilizing the electron-rich axial ligand (nucleophile) in the transition state (mechanism for styrene oxidation is shown below Figure 3.15).

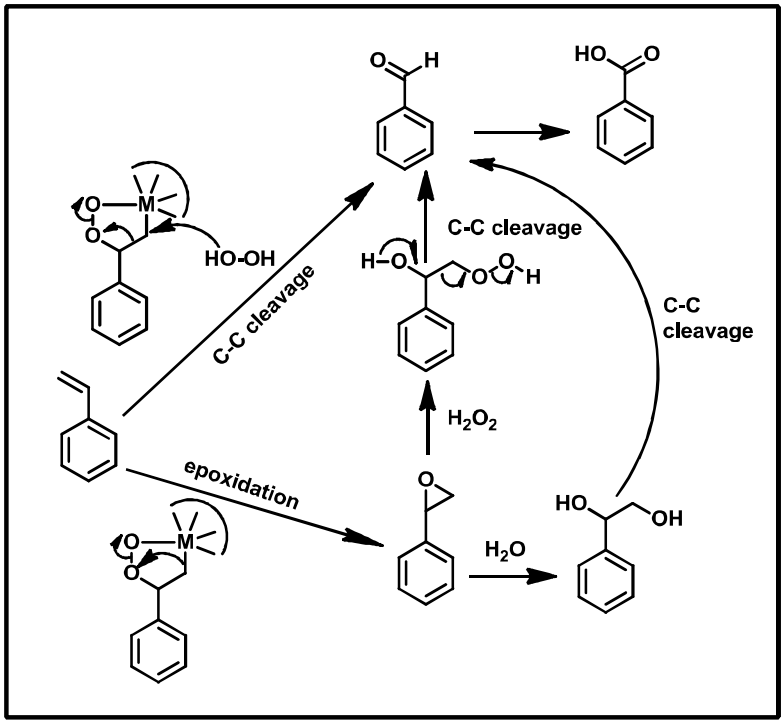

Figure 3.15: A mechanism for the oxidation of styrene.[75]

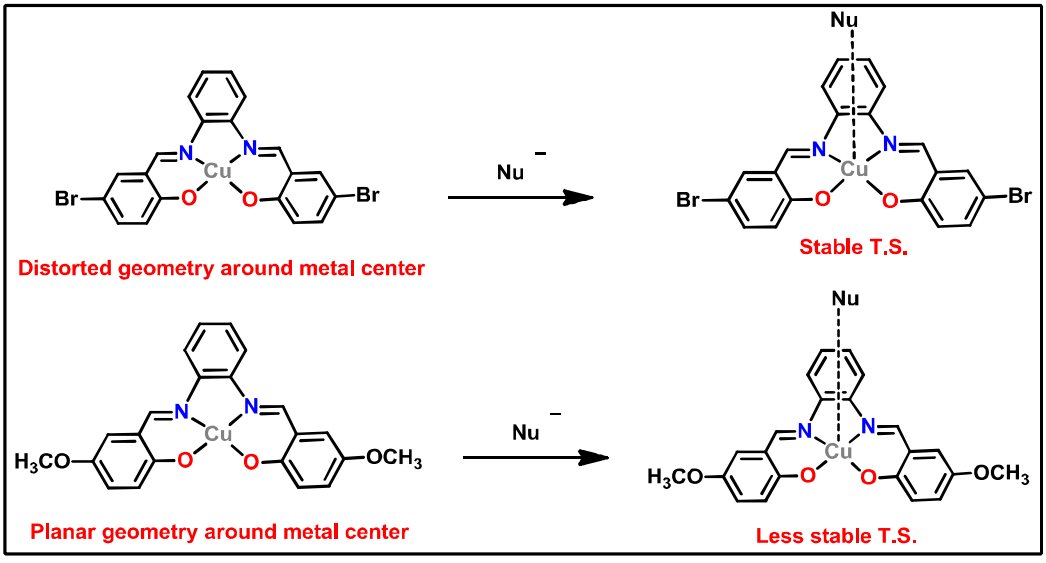

Figure 3.16: Effect of substituent's on the geometry of complex around the metal and its effect on the transition state (T.S.) during the nucleophilic attack.

In the series, the CuL3 complex shows slightly lesser reactivity than expected, the reason could be the low solubility of the complex in the reaction medium. Encapsulation of CuL3 complexes inside the supercage further enhances the degree of distortion and makes the metal, even more, electron-deficient and consequently more reactive. The performance of the catalysts is well understood, as the main decisive factors like an electronic factor of electron withdrawing groups and space constraint imposed by zeolite Y under encapsulation are additive to each other and working in synergistic fashion here. Free state CuL2 and CuL5 complexes are not as much reactive since they may exist in the dimeric form in their solution states,[66] or because of the less receptive copper metal center for the nucleophillic attack of H_2O_2 since both the complexes have electron-donating groups attached on the phenyl rings. However, these complexes when encapsulated in zeolite Y have shown very exciting catalytic behavior. Among all, the most striking observation is with CuL5 complex as when encapsulated it has shown remarkable enhancement in reactivity for the above-mentioned reaction. On encapsulation, the TON of CuL5 catalyst increases from 187 to 3543. Hence the competence of the heterogeneous system is mainly driven by the electron deficiency of the metals administered by the steric factor, which actually opposes the original electronic factor of substituent groups (-OCH_3). The electron deficient character of the metals via steric constraint imposed by the topology of zeolite supercage dominates and enhances the reactivity as the addition of two -OCH_3 groups on phenyl rings makes the complex largest in the series and hence more distorted inside the rigid host cavity of zeolite Y. Consequently, the metal center becomes more electropositive, showing extraordinarily higher catalytic activities. CuL2 complex having electron-donating substituent groups (-OH) and with moderate molecular dimensions when encapsulated, are not such efficient catalysts as CuL5 complex in its encapsulated state. Encapsulated CuL2 complex shows enhancement of catalytic activity as steric constraints obscure the inherent electron effect. Overall catalytic data have illustrated the reactivity of free state copper Schiff-base complexes driven by only the electronic factor and hence, the trend of reactivity follows the order as CuL1 >CuL3 >CuL2 >CuL5. After encapsulation of complexes in the zeolite Y, molecular dimensions and extent of distortion of the guest complexes mainly drive the reactivity order. The catalytic reactivity order in the encapsulated state for the copper salophen complexes, therefore, becomes CuL5 >CuL3 >CuL2 >CuL1. The experimentally observed blue shift of d-d transition in electronic spectra also support the above catalytic order of the encapsulated complexes; larger is the blue shift, more will be the catalytic activity. A further interesting observation, while comparing the catalytic activities of salophen with that of salen complexes in both

states, is the reactivity of copper salen and salophen complexes are approximately comparable, however, that is not the case for encapsulated analogues. Only Cu(II) salen and CuL1 complexes show comparable reactivity; however other substituted copper salophen complexes are definitely better catalysts than the corresponding salen complexes.[76] Larger is the molecular dimensions of a complex; more is the reactivity after the encapsulation in the zeolite Y towards the styrene oxidation reaction.

3.3 CONCLUSION

Zeolite framework certainly provides a route to design the heterogeneous catalyst with customized reactivity by the encapsulation process. Rigid walls of framework impose space restraint on the guest complex forcing the guest complex to adopt distorted structure. Such alteration in the structure of the complex plays a crucial role in the modified reactivity of the system. The observed blue shift in a d-d transition in electronic spectra signifies the alternation in the metal d orbitals energy levels, which is certainly an effect of the altered coordination sphere around the metal center. This adaptation of nearly planar geometry finally leads to the non-planar geometry and therefore, the metal center becomes more electropositive. Non-planar geometry impedes the conjugation around the metal center. XPS studies also support the enhanced electropositive character of the metal in the encapsulated complexes as the Cu (2p) XPS signal for the encapsulated complexes shifts towards higher binding energy. The more electropositive character of the metal center, more susceptible it will be for the nucleophilic attack of H_2O_2. It is obvious that the larger molecular dimension leads to more deformation in the geometry of complex and as an effect the creation of more active metal center in the encapsulated state of the complex. Comparative catalytic studies of these host-guest systems provide an interesting correlation between modified structural aspects and modified reactivity of the guest complexes, and so it can be concluded, as the degree of distortion in the structure of the encapsulated guest complex is the key point for the remarkable modified catalytic activity of the systems.

3.4 REFERENCES

1. N. Y. Chen and W. E. Garwood, *J. Catal.*, 1978, **52**, 453-458.
2. S. Deshpande, D. Srinivas and P. Ratnasamy, *J. Catal.*, 1999, **188**, 261-269.
3. J. R. Anderson, K. Foger, T. Mole, R. A. Rajadhyaksha and J. V. Sanders, *J. Catal.*, 1979, **58**, 114-130.
4. M. R. Maurya, A. K. Chandrakar and S. Chand, *J. Mol. Catal. A: Chem.*, 2007, **274**, 192-201.
5. C. Jin, W. Fan, Y. Jia, B. Fan, J. Ma and R. Li, *J. Mol. Catal. A: Chem.*, 2006, **249**, 23-30.
6. K. J. Balkus and A. G. Gabrielov, in *Inclusion Chemistry with Zeolites: Nanoscale Materials by Design*, eds. N. Herron and D. R. Corbin, Springer Netherlands, Dordrecht, 1995, DOI: 10.1007/978-94-011-0119-6_6, pp. 159-184.
7. K. K. Bania and R. C. Deka, *J. Phys. Chem. C*, 2013, **117**, 11663-11678.
8. E. R. Shilpa and V. Gayathri, *J. Environ. Chem. Eng.*, 2016, **4**, 4194-4206.
9. M. Salavati-Niasari, *J. Mol. Catal. A: Chem.*, 2005, **229**, 159-164.
10. M. Salavati-Niasari and A. Sobhani, *Journal of Molecular Catalysis A: Chemical*, 2008, **285**, 58-67.
11. M. Salavati-Niasari, *J. Mol. Catal. A: Chem.*, 2008, **283**, 120-128.
12. M. Salavati-Niasari and F. Davar, *Inorg. Chem. Commun.*, 2006, **9**, 263-268.
13. J. Zhu, Z. Kónya, V. F. Puntes, I. Kiricsi, C. X. Miao, J. W. Ager, A. P. Alivisatos and G. A. Somorjai, *Langmuir*, 2003, **19**, 4396-4401.
14. D. E. De Vos, M. Dams, B. F. Sels and P. A. Jacobs, *Chem. Rev.*, 2002, **102**, 3615-3640.
15. C.-Y. Sun, X.-L. Wang, X. Zhang, C. Qin, P. Li, Z.-M. Su, D.-X. Zhu, G.-G. Shan, K.-Z. Shao, H. Wu and J. Li, *Nat. Commun.*, 2013, **4**, 2717.
16. P. Ling, J. Lei, L. Zhang and H. Ju, *Anal. Chem.*, 2015, **87**, 3957-3963.
17. D. T. Genna, A. G. Wong-Foy, A. J. Matzger and M. S. Sanford, *J. Am. Chem. Soc.*, 2013, **135**, 10586-10589.
18. Q. Yao and Y. Zhang, *Angew. Chem., Int. Ed. Engl.*, 2003, **42**, 3395-3398.
19. I. J. B. Lin and C. S. Vasam, *J. Organomet. Chem*, 2005, **690**, 3498-3512.
20. M. Benjamin, D. Manoj, K. Thenmozhi, P. R. Bhagat, D. Saravanakumar and S. Senthilkumar, *Biosens. Bioelectron.*, 2017, **91**, 380-387.
21. M. Salavati-Niasari, P. Salemi and F. Davar, *J. Mol. Catal. A: Chem.*, 2005, **238**, 215-222.
22. M. Cinouini, S. Colonna, H. Molinari, F. Montanari and P. Tundo, *J. Chem. Soc., Chem. Commun.*, 1976, DOI: 10.1039/C39760000394, 394-396.
23. X. Zuwei, Z. Ning, S. Yu and L. Kunlan, *Science*, 2001, **292**, 1139-1141.
24. M. R. Maurya, A. K. Chandrakar and S. Chand, *J. Mol. Catal. A: Chem.*, 2007, **263**, 227-237.
25. C. Bowers and P. K. Dutta, *Journal of Catalysis*, 1990, **122**, 271-279.
26. A. A. Valente and J. Vital, in *Studies in Surface Science and Catalysis*, eds. H. U. Blaser, A. Baiker and R. Prins, Elsevier, 1997, vol. 108, pp. 461-468.
27. M. Salavati-Niasari, *Microporous Mesoporous Mater.*, 2006, **95**, 248-256.
28. M. Salavati-Niasari, *Inorg. Chem. Commun.*, 2006, **9**, 628-633.
29. M. Salavati-Niasari and M. Bazarganipour, *Catal. Commun.*, 2006, **7**, 336-343.
30. M. Salavati-Niasari, E. Zamani, M. R. Ganjali and P. Norouzi, *J. Mol. Catal. A: Chem.*, 2007, **261**, 196-201.
31. F. Bedioui, *Coord. Chem. Rev.*, 1995, **144**, 39-68.
32. S.-N. Masoud, *Chem. Lett.*, 2005, **34**, 1444-1445.
33. M. Salavati-Niasari, *Inorg. Chem. Commun.*, 2005, **8**, 174-177.
34. S.-N. Masoud, *Chem. Lett.*, 2005, **34**, 244-245.
35. M. Salavati-Niasari, *Inorg. Chem. Commun.*, 2004, **7**, 963-966.
36. M. Salavati-Niasari, *Polyhedron*, 2009, **28**, 2321-2328.

37. R. F. Parton, I. F. J. Vankelecom, M. J. A. Casselman, C. P. Bezoukhanova, J. B. Uytterhoeven and P. A. Jacobs, *Nature*, 1994, **370**, 541-544.
38. M. R. Maurya, A. K. Chandrakar and S. Chand, *J. Mol. Catal. A: Chem.* , 2007, **274**, 192-201.
39. M. R. Maurya, A. K. Chandrakar and S. Chand, *J. Mol. Catal. A: Chem.*, 2007, **270**, 225-235.
40. B. Neelam, N. Fehmida, B. Alok, B. Sudha and A. Amir, *Eur. J. Med. Chem.*, 2000, **35**, 481-486.
41. M. Maurya, S. Titinchi, S. Chand and I. Mishra, *J. Mol. Catal. A: Chem.*, 2002, **180**, 201-209.
42. M. R. Maurya, S. J. Titinchi and S. Chand, *J. Mol. Catal. A: Chem.*, 2003, **201**, 119-130.
43. D. R. Godhani, H. D. Nakum, D. K. Parmar, J. P. Mehta and N. C. Desai, *J. Mol. Catal. A: Chem.*, 2017, **426**, 223-237.
44. M. Martis, K. Mori and H. Yamashita, *Dalton Trans.*, 2014, **43**, 1132-1138.
45. S. Seelan and A. K. Sinha, *Appl. Catal., A*, 2003, **238**, 201-209.
46. S. Bhar and R. Ananthakrishnan, *Photochem. Photobiol. Sci.*, 2017, **16**, 1290-1300.
47. M. Sharma, B. Das, G. V. Karunakar, L. Satyanarayana and K. K. Bania, *J. Phys. Chem. C*, 2016, **120**, 13563-13573.
48. G. R. Reddy and S. Balasubramanian, *Microporous Mesoporous Mater.*, 2016, **231**, 207-215.
49. G. Ramanjaneya Reddy, S. Balasubramanian and K. Chennakesavulu, *J. Mater. Chem. A*, 2014, **2**, 15598-15610.
50. S. J. Titinchi, G. Von Willingh, H. S. Abbo and R. Prasad, *Catal. Sci. Technol.*, 2015, **5**, 325-338.
51. A. Choudhary, B. Das and S. Ray, *Dalton Trans.*, 2016, **45**, 18967-18976.
52. M. Salavati-Niasari, Z. Salimi, M. Bazarganipour and F. Davar, *Inorg. Chim. Acta*, 2009, **362**, 3715-3724.
53. M. M. Bhadbhade and D. Srinivas, *Inorg. Chem.*, 1993, **32**, 6122-6130.
54. K. O. Xavier, J. Chacko and K. K. Mohammed Yusuff, *Appl. Catal., A*, 2004, **258**, 251-259.
55. S. Sharma, S. Sinha and S. Chand, *Ind. Eng. Chem. Res.*, 2012, **51**, 8806-8814.
56. C. R. Jacob, S. P. Varkey and P. Ratnasamy, *Appl. Catal., A*, 1998, **168**, 353-364.
57. G. R. Reddy, S. Balasubramanian and K. Chennakesavulu, *J. Mater. Chem. A*, 2014, **2**, 19102-19102.
58. A. Choudhary, B. Das and S. Ray, *Dalton Trans.*, 2015, **44**, 3753-3763.
59. W. H. Quayle, G. Peeters, G. L. De Roy, E. F. Vansant and J. H. Lunsford, *Inorg. Chem.*, 1982, **21**, 2226-2231.
60. K. K. Bania, D. Bharali, B. Viswanathan and R. C. Deka, *Inorg. Chem.*, 2012, **51**, 1657-1674.
61. R. Ganesan and B. Viswanathan, *J. Phys. Chem. B*, 2004, **108**, 7102-7114.
62. G. Ramanjaneya Reddy, S. Balasubramanian and K. Chennakesavulu, *J. Mater. Chem. A*, 2014, **2**, 15598-15610.
63. S. L. Hailu, B. U. Nair, M. Redi-Abshiro, I. Diaz, R. Aravindhan and M. Tessema, *Chin. J. Catal.*, 2016, **37**, 135-145.
64. B. Kumar Kundu, V. Chhabra, N. Malviya, R. Ganguly, G. S. Mishra and S. Mukhopadhyay, *Microporous Mesoporous Mater.*, 2018, **271**, 100-117.
65. S. Koner, *Chem. Commun.*, 1998, DOI: 10.1039/A707681I, 593-594.
66. M. M. Bhadbhade and D. Srinivas, *Inorganic Chemistry*, 1993, **32**, 6122-6130.
67. L. Gomes, E. Pereira and B. de Castro, *J. Chem. Soc., Dalton Trans.*, 2000, DOI: 10.1039/A908330H, 1373-1379.
68. N. Grover, M. Sankar, Y. Song and K. M. Kadish, *Inorg. Chem.*, 2016, **55**, 584-597.
69. M. R. Maurya, B. Singh, P. Adão, F. Avecilla and J. Costa Pessoa, *Eur. J. Inorg. Chem.*, 2007, **2007**, 5720-5734.
70. S. Rayati, S. Zakavi, M. Koliaei, A. Wojtczak and A. Kozakiewicz, *Inorg. Chem. Commun.*, 2010, **13**, 203-207.
71. S. J. J. Titinchi, G. Von Willingh, H. S. Abbo and R. Prasad, *Catal. Sci. Technol.*, 2015, **5**, 325-338.

72. M. R. Maurya, B. Singh, P. Adão, F. Avecilla and J. Costa Pessoa, *Eur. J. Inorg. Chem.*, 2007, **2007**, 5720-5734.
73. A. Boettcher, H. Elias, E. G. Jaeger, H. Langfelderova, M. Mazur, L. Mueller, H. Paulus, P. Pelikan, M. Rudolph and M. Valko, *Inorg. Chem.*, 1993, **32**, 4131-4138.
74. M. M. Bhadbhade and D. Srinivas, *Inorganic Chemistry*, 1993, **32**, 6122-6130.
75. T. A. G. Duarte, A. C. Estrada, M. M. Q. Simoes, I. C. M. S. Santos, A. M. V. Cavaleiro, M. G. P. M. S. Neves and J. A. S. Cavaleiro, *Catal. Sci. Technol.*, 2015, **5**, 351-363.
76. S. Kumari, A. Choudhary and S. Ray, *Appl. Organomet. Chem.*, 2019, **33**, e4765.